Journal of Applied Physics

RESEARCH ARTICLE | AUGUST 15 2025

Effects of Ni irradiation on electron–phonon coupling and flux pinning in MgB_2 film via Raman spectroscopy

Duong T. T. Nhan ; An T. Pham; Tien Le ; Won-Nam Kang; Dzung T. Tran ; Hong-Gu Lee ; Jungseek Hwang ; Nguyen Hoang Nam ; Ha H. Pham ; Khoi M. C. Pham ; Pham Ngoc Thao; Phan Hai ; Soo-Kien Chen ; M. Dogruer ; Kieu Xuan Thuy; Duc H. Tran

J. Appl. Phys. 138, 073901 (2025)
https://doi.org/10.1063/5.0285394

Articles You May Be Interested In

AIP Publishing

Journal of Applied Physics | ARTICLE | pubs.aip.org/aip/jap

Effects of Ni irradiation on electron–phonon coupling and flux pinning in MgB_2 film via Raman spectroscopy

Cite as: J. Appl. Phys. **138**, 073901 (2025); doi: 10.1063/5.0285394
Submitted: 14 June 2025 · Accepted: 30 July 2025 ·
Published Online: 15 August 2025

View Online Export Citation CrossMark

Duong T. T. Nhan,[1] An T. Pham,[1] Tien Le,[2] Won-Nam Kang,[3] Dzung T. Tran,[3] Hong-Gu Lee,[3] Jungseek Hwang,[3] Nguyen Hoang Nam,[1] Ha H. Pham,[1] Khoi M. C. Pham,[1] Pham Ngoc Thao,[4] Phan Hai,[5] Soo-Kien Chen,[6] M. Dogruer,[7] Kieu Xuan Thuy,[1] and Duc H. Tran[1,a)]

AFFILIATIONS

[1]Nano & Energy Center, Faculty of Physics, University of Science, Vietnam National University, Hanoi 100000, Vietnam
[2]Department of General Education, University of Science and Technology of Hanoi, Vietnam Academy of Science and Technology, 18 Hoang Quoc Viet, Nghia Do, Hanoi 100000, Vietnam
[3]Department of Physics, Sungkyunkwan University, Suwon 16419, South Korea
[4]Faculty of Electronics and Telecommunications, VNU University of Engineering and Technology, Hanoi 100000, Vietnam
[5]Faculty of Engineering Physics and Technology, Vietnam National University, Hanoi 100000, Vietnam
[6]Department of Physics, Faculty of Science, University Putra Malaysia, 43400 Serdang, Selangor, Malaysia
[7]Department of Medical Services and Techniques, Bolu Abant Izzet Baysal University, Bolu, Turkey

[a)]**Author to whom correspondence should be addressed:** dhtran@hus.edu.vn

ABSTRACT

Effects of Ni-ion irradiation on the structural and flux-pinning properties of MgB_2 films were investigated with particular importance on the role of Raman spectroscopy. MgB_2 films (∼400 nm thick) were fabricated on *c*-cut Al_2O_3 substrates using a hybrid physicochemical vapor deposition technique and irradiated with 1 MeV Ni ions at doses ranging from 3×10^{13} to 9×10^{13} ions/cm^2. X-ray diffraction (XRD) and Raman spectroscopy were examined to characterize the crystallinity and electron–phonon coupling (EPC) in the films, while magnetization measurements provided insights into the superconducting properties. The XRD results confirmed that all films were highly *c*-axis oriented, and the *c*-axis lattice constant slightly increased with increased Ni-ion dose. Raman spectra revealed significant changes in the E_{2g} phonon mode, including shifts in peak positions and broadened FWHM (full-width at half-maximum), indicative of EPC degradation and the introduction of lattice disorder at an atomic scale. The decrease in the critical temperature (T_c) with increasing Ni-ion dose was correlated with these spectroscopic changes. The self-field critical current density (J_c) of the pristine MgB_2 film was well maintained to be 4×10^6 A/cm^2 at 20 K. Above the field of ∼2.5 T, the J_c was observed to clearly enhance and reach a maximum at a Ni-ion dose of 5×10^{13} ions/cm^2, and J_c was maintained ∼10^3 A/cm^2 at the field of ∼3.7 T. The observations might reveal the dominance of core point pinning, which resulted from the Ni-ion irradiation.

I. INTRODUCTION

MgB_2 superconductors were discovered in 2001.[1] They exhibit a superconducting transition temperature (T_c) of approximately 39 K, opening extensive research into superconductivity and its applications[2–4] The advantages of MgB_2 include its simple hexagonal crystal structure, a relatively large coherence length $\xi_{ab}(0)$ of around 8.5 nm,[5] high critical current density (J_c), and high upper critical field (H_{c2}). Additionally, MgB_2 is a lightweight and cost-effective material, making it attractive for power-related applications, such as superconducting power cables, grid-scale fault current limiters, and energy-efficient transformers in modern electrical grids. However, the critical current density drops significantly under applied magnetic fields due to weak flux pinning. To mitigate this issue, various ion irradiation techniques have been employed to introduce controlled defects into MgB_2 thin films. For instance, Sn^{2+} ion irradiation has been shown to significantly enhance in-field J_c and H_{c2}, despite a slight decrease in T_c.[6] Similarly, carbon-ion irradiation introduces defects through nuclear stopping, resulting in c-axis lattice expansion and increased residual resistivity, both of which correlate with improved H_{c2} and in-field J_c.[7] Numerous studies have aimed to enhance J_c by analyzing vortex-pinning mechanisms, which include point pinning, surface pinning, and Δκ pinning. Each mechanism contributes differently depending on the applied magnetic field: surface pinning is more effective at low fields, while point and Δκ pinning dominate at higher fields.[8] Homogeneous distribution of pinning centers throughout the superconducting matrix is particularly effective in enhancing J_c. Efforts to improve flux pinning in MgB_2 films through non-magnetic ion irradiation, such as proton,[9] neutron,[10] oxygen,[11–13] tin,[8] helium,[14] and carbon[15] ions, have generally produced positive results, with enhanced J_c and dominance of point-like pinning confirmed. More recently, research attention has shifted toward the use of magnetic ions. While Fe-ion irradiation has been performed on MgB_2 films,[16,17] those studies primarily focused on local structure and optical properties rather than directly on flux-pinning behavior. Thus, the effect of magnetic-ion irradiation on flux-pinning properties remains relatively unexplored.

In this study, the irradiation of MgB_2 films with Ni ions investigates how defects and lattice distortions affect the structure of material and superconducting properties. Ni-ion irradiation causes lattice expansion and significant degradation of crystallinity, as shown by broadening of XRD peaks and increased tensile strain confirmed by Williamson–Hall analysis. While the critical temperature (T_c) decreases notably with increasing ion dose and electron–phonon coupling weakens, flux pinning is importantly enhanced. Raman spectroscopy reveals shifts in phonon modes consistent with increased lattice disorder. The critical current density (J_c) improves significantly in high magnetic fields for intermediate irradiation doses, corresponding with a transition to stronger, defect-driven pinning mechanisms. Increased surface roughness and grain boundary degradation observed by AFM further support the formation of effective pinning centers.

II. EXPERIMENTS

We fabricated ∼400 nm-thick MgB_2 films on *c*-cut Al_2O_3 substrates using the hybrid physicochemical vapor deposition (HPCVD) technique under previously reported fabrication conditions.[8] Ni-ion irradiation was carried out using the HUS-5SDH-2 tandem Pelletron accelerator at VNU University of Science, Vietnam. The Ni-ion beam energy was fixed at 1 MeV, and ion doses of 3×10^{13}, 5×10^{13}, 7×10^{13}, and 9×10^{13} ions/cm^2 were applied. The corresponding MgB_2 film samples were labeled as pristine, 3×10^{13}, 5×10^{13}, 7×10^{13}, and 9×10^{13}, respectively. The use of 1 MeV Ni-ion energy enabled deep and relatively uniform defect formation within the MgB_2 films, promoting point-like defects that enhance flux pinning while minimizing excessive lattice damage that could degrade superconductivity. The mean projected range (R_p) is defined as the average distance an ion travels along the initial beam direction before coming to rest in the target) of the Ni ions was estimated using the Monte Carlo simulation program SRIM (Stopping and Range of Ions in Matter).[18,19] Irradiation was performed with the Ni-ion beam perpendicular to the film surface, aligning with the crystallographic c-axis. The magnetic field applied during magnetization and critical current density (J_c) measurements was also oriented perpendicular to the film surface to ensure alignment with the c-axis. Crystallinity of the MgB_2 films was characterized by X-ray diffraction (XRD), while room-temperature Raman spectroscopy was performed using a MAPLE II spectrometer with a 532 nm green laser. The superconducting transition temperature (T_c) was determined from magnetization vs temperature (M–T) measurements at 100 Oe. Critical current density (J_c) values at 5 and 20 K were derived from magnetization vs field (M–H) curves using Bean's model, $J_c = \Delta M/r$,[8] where r is the sample radius and ΔM is the magnetization difference at each applied field. All M–T and M–H measurements were conducted using a Physical Property Measurement System (Quantum Design, EverCool, Model 6000) with the field applied perpendicular to the film surface.

III. RESULTS AND DISCUSSION

The Ni-ion irradiation process on an MgB_2 film deposited on a *c*-cut Al_2O_3 substrate was simulated using the SRIM program.[18,19] Based on input parameters of 1 MeV Ni-ion energy and an MgB_2 density of 2.57 g/cm^3, the R_p was found to exceed 900 nm, as shown in Fig. 1. Given the MgB_2 film thickness of approximately 400 nm in this study, most Ni ions are expected to pass entirely through the film and stop in the substrate. As shown in Fig. 1(b), the number of vacancies generated within the film remains relatively constant throughout its thickness. These results indicate that Ni-ion tracks effectively create line defects and lattice distortion within the MgB_2 layer.[8]

The XRD patterns of the pristine and Ni-irradiated MgB_2 films with different ion doses are shown in Fig. 2(a). All films exhibit high c-axis orientation, as indicated by the presence of only two sharp and dominant diffraction peaks: (0001) and (0002). No impurity peaks were observed. To determine changes in crystallinity, the full width at half maximum (FWHM) of the (0002) peak was compared before and after Ni irradiation, as shown in Fig. 2(b). The FWHM of the (0002) peak increased from 0.257° in the pristine film to 0.479° in the irradiated samples, demonstrating degradation in crystallinity due to ion-induced lattice disorder. In addition, a slight shift of the (0001) and (0002) peaks toward lower 2θ values was observed in all irradiated films, indicating an expansion of the c-axis lattice parameter. Among the two peaks, the (0002) reflection was selected for lattice parameter analysis due to its approximately six times higher intensity compared to the (0001) peak. The c-axis lattice constant was calculated using the following relation:

$$c = d\sqrt{h^2 + k^2 + l^2}.$$

The crystal structure of MgB_2 is hexagonal, and the (0002) reflection corresponds to Miller indices $[h\ k-(h+k)\ l]$, where $h = 0$, $k = 0$, and $l = 2$. The *c*-axis lattice constant, calculated from

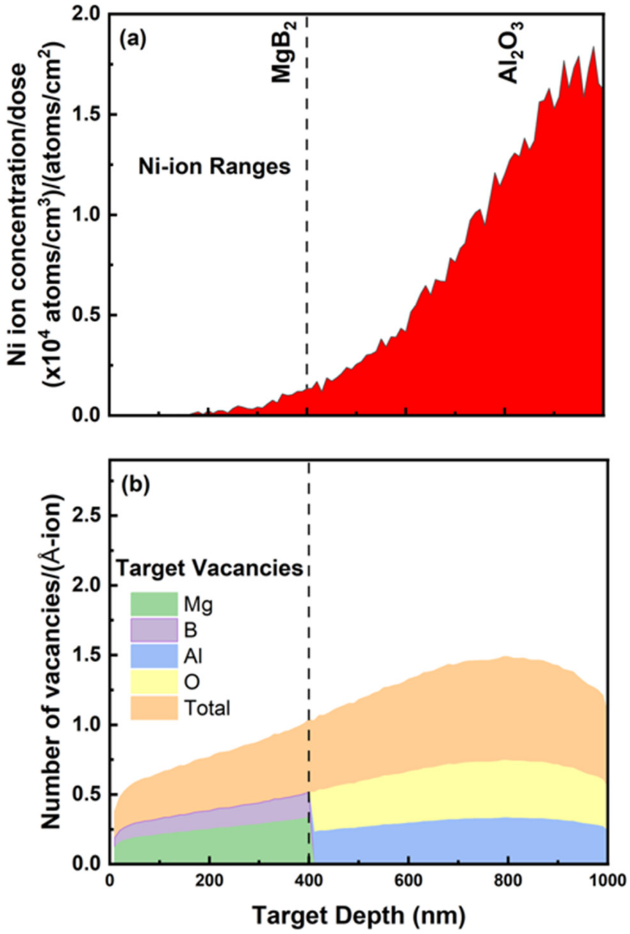

FIG. 1. (a) Mean projected range of 1 MeV nickel ions irradiated on the MgB_2 film deposited on the *c*-cut Al_2O_3 substrate and (b) the depth profile of the number of target vacancies generated by 1 MeV Ni-ion irradiation.

the (0002) peak, is given in Table I. It was found to increase slightly from 3.521 Å in the pristine MgB_2 film to 3.550 Å with increasing Ni-ion dose. Geometrically, irradiation was performed nearly along the c-axis direction of the MgB_2 films. The collision of Ni ions with Mg and B atoms along this direction may have contributed to *c*-axis elongation, consistent with previous reports.[20,21] The formation of defects and lattice disorder during Ni-ion irradiation may influence scattering between the π and σ bands in MgB_2, potentially altering its superconducting properties. The gradual shift of the (0002) XRD peak toward lower 2θ angles with increasing Ni-ion dose indicates tensile strain (ε) within the films. This observation is quantitatively supported by increasing ε values obtained from Williamson–Hall analysis, as shown in Table I. Tensile strain, arising from defect-induced lattice expansion under Ni irradiation, likely contributes to enhanced grain boundary pinning, while avoiding excessive stress accumulation that could otherwise degrade the film structural integrity.

To investigate the variation in superconductivity of MgB_2 films with increasing Ni-ion doses, the zero-field cooling (ZFC) and field cooling (FC) magnetization vs temperature (M–T) curves were measured. The lower critical field (H_{c1}) of MgB_2 is reported to be around 2800 Oe, so the applied field along the *c*-axis in the experiment was set to 10 Oe. The ZFC and FC curves are shown in Fig. 3. The superconducting state was established as the temperature dropped below the critical temperature (T_c). In the ZFC mode, the 10 Oe applied field was completely excluded from the MgB_2 films, resulting in diamagnetism below T_c. In the FC mode, the 10 Oe field was trapped in the form of vortices inside the films, leading to weaker magnetization compared to the ZFC mode. T_c was determined as the temperature at the point where the normalized M–T curves merged.[8,12,22] The values of T_c for each Ni-ion dose are given in Table I. It can be observed that T_c decreased from 39.56 K for the pristine MgB_2 film to 32.50 K for the film irradiated with 9×10^{13} Ni ions/cm^2. The decrease in T_c in superconductors is often attributed to impurities, crystal disorders, and defects.[23–25] Therefore, the defects and lattice disorders induced by Ni-ion irradiation are likely the primary cause of the reduction in T_c for the irradiated MgB_2 films.

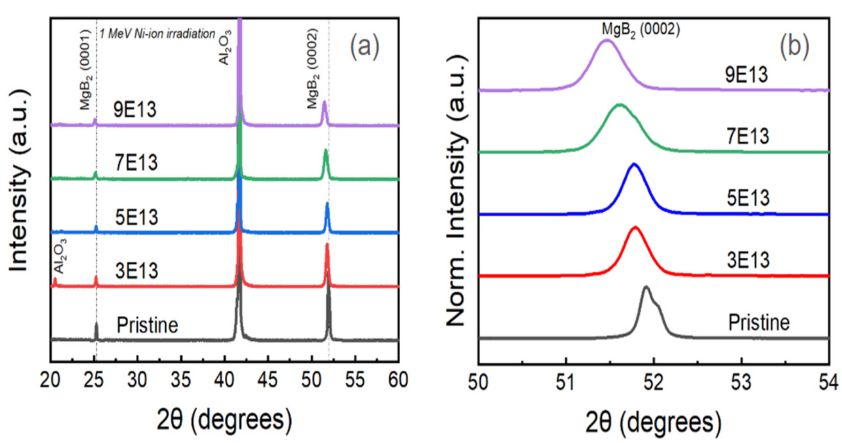

FIG. 2. (a) X-ray diffraction (XRD) diagram of the pristine and Ni-ion irradiated MgB_2 films. All MgB_2 films were highly *c*-axis oriented with the absence of impurity phase, and (b) the (0002) MgB_2 peaks were found to systematically shift to a lower value of 2*θ*.

TABLE I. Values of T_c, Raman peak centers, FWHM of E_{2g}, electron–phonon coupling, Θ_D, and strain of the pristine and Ni-irradiated MgB_2 films.

Samples	T_c (K)	c-axis (Å)	ω_1 (cm^{-1})	ω_2 (E_{2g}) (cm^{-1})	ω_3 (cm^{-1})	FWHM (E_{2g}) (cm^{-1})	EPC (λ)	Θ_D (K)	ε (%)
Pristine	39.56	3.5210	421.85	598.60	748.62	213.22	1.049	700.83	0.191
3×10^{13}	36.25	3.5327	415.61	572.57	729.45	214.24	1.014	678.46	0.388
5×10^{13}	35.01	3.5305	419.11	568.84	731.62	205.57	0.994	678.17	0.538
7×10^{13}	33.75	3.5423	406.07	566.92	731.51	207.76	0.978	671.67	0.633
9×10^{13}	32.50	3.5500	402.52	560.33	730.57	198.16	0.962	666.07	1.084

Among the optical phonon modes of MgB_2 (namely, E_{2g}, E_{1u}, B_{1g}, and A_{2u}), the E_{2g} mode was uniquely identified as the only first-order Raman-active mode in the pristine crystal structure.[26–28] The E_{1u}, B_{1g}, and A_{2u} modes tend to become dominant in the presence of crystal defects or impurities.[29–32] Therefore, Raman spectra can provide deep insights into electron–phonon coupling (EPC), crystal defects, lattice disorder, and impurities. Figure 4(a) shows the room-temperature Raman spectra of pristine and Ni-irradiated MgB_2 films, which exhibit a clear dependence on Ni-ion dose. To quantitatively analyze the spectra, Gaussian fitting was applied to the experimental data. All spectra were well fitted with three peaks: ω_1, ω_2, and ω_3. Among these, the ω_1 peak ($\sim$420 cm^{-1}) had low intensity and limited influence and thus was not discussed in detail. According to previous studies, the E_{2g} mode in the hexagonal structure of MgB_2 corresponds to the central peak ω_2, while the ω_1 and ω_3 peaks are associated with lattice distortion.[26–28,33,34] Two key features of the ω_2 peak, the peak position and its FWHM, are particularly important indicators of EPC. These parameters are listed in Table I and shown in Figs. 4(b) and 4(c). The E_{2g} peak position, initially located at $\sim$598 cm^{-1} for the pristine film, gradually shifted to lower values with increasing Ni-ion dose, reaching a minimum of 560 cm^{-1} for the film irradiated with 9×10^{13} ions/cm^2. The FWHM of the E_{2g} peak, which was $\sim$213 cm^{-1} in the pristine film, slightly decreased to $\sim$198 cm^{-1} in the most heavily irradiated sample. A high FWHM ($\sim$200 cm^{-1}) is generally associated with strong EPC,[30,31,35] and the observed decrease may be partially related to the reduction in T_c with increasing defect concentration induced by Ni-ion irradiation.[29]

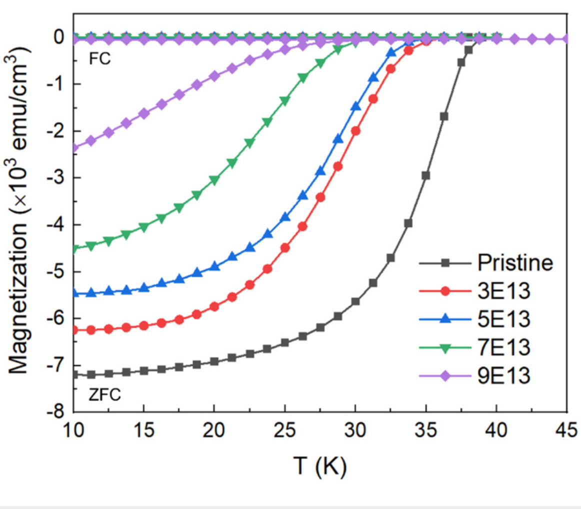

FIG. 3. Zero-field cooled (ZFC) and field-cooled (FC) magnetization vs temperature (M–T) curves of the pristine and Ni-ion irradiated MgB_2 films. The superconducting transitions were observed for all films, and T_c was defined as the temperature of the merging point in the M–T curves.

Although the E_{2g} peak obviously broadened, an additional peak well fitted by ω_3 became dominant. This peak growth has previously been observed in MgB_2 samples subjected to chemical substitution or irradiation.[17,21,29,36] In strongly disordered or crystal-defect systems, the momentum-selection rule can lead to Raman scattering from a broader range of phonon modes, revealing features of the phonon density of states (PDOS).[26,34] In our study, lattice distortion and strain in the MgB_2 films were induced by Ni-ion irradiation. The increasing prominence of the ω_3 peak with higher Ni-ion doses may indicate the emergence of PDOS-related features in the Raman spectra, which likely contribute to the degradation of superconductivity in the MgB_2 films.

The relation between T_c, phonon frequency, and EPC can be expressed by the McMillan formula with the revision of Allen–Dynes[37] as

$$T_c = \frac{\langle\omega\rangle}{1.2}\exp\left(-\frac{1.04(1+\lambda)}{\lambda-\mu^*(1+0.62\lambda)}\right),$$

where the average phonon frequency $\langle\omega\rangle$ is estimated as $\langle\omega\rangle = (\omega_1 \times \omega_2^2 \times \omega_3)^{0.25}$,[38,39] μ^* is the Coulomb pseudopotential (taken as equal to 0.13),[40] and λ is the EPC constant. Another parameter, the Debye temperature (Θ_D), may be deduced from the $\langle\omega\rangle$ through the relation

$$\Theta_D = \frac{\langle\omega\rangle}{1.2} \times 1.45.$$

The obtained fitting parameters are listed in Table I. The EPC value for the pristine MgB_2 film was 1.049, and it monotonically decreased to 0.962 as the Ni-ion dose increased to 9×10^{13} ions/cm^2. This reduction in EPC is linked to the observed decrease in T_c, as the electron–phonon coupling plays a crucial role in determining the superconducting transition temperature. The electron–phonon interaction was explained using the Bardeen–Cooper–Schrieffer (BCS) theory, where the attraction between two electrons is mediated by the exchange of virtual phonons. In addition, MgB_2 is known to exhibit two superconducting gaps associated with the σ- and π-bands. The EPC for the σ-band and π-band was calculated to

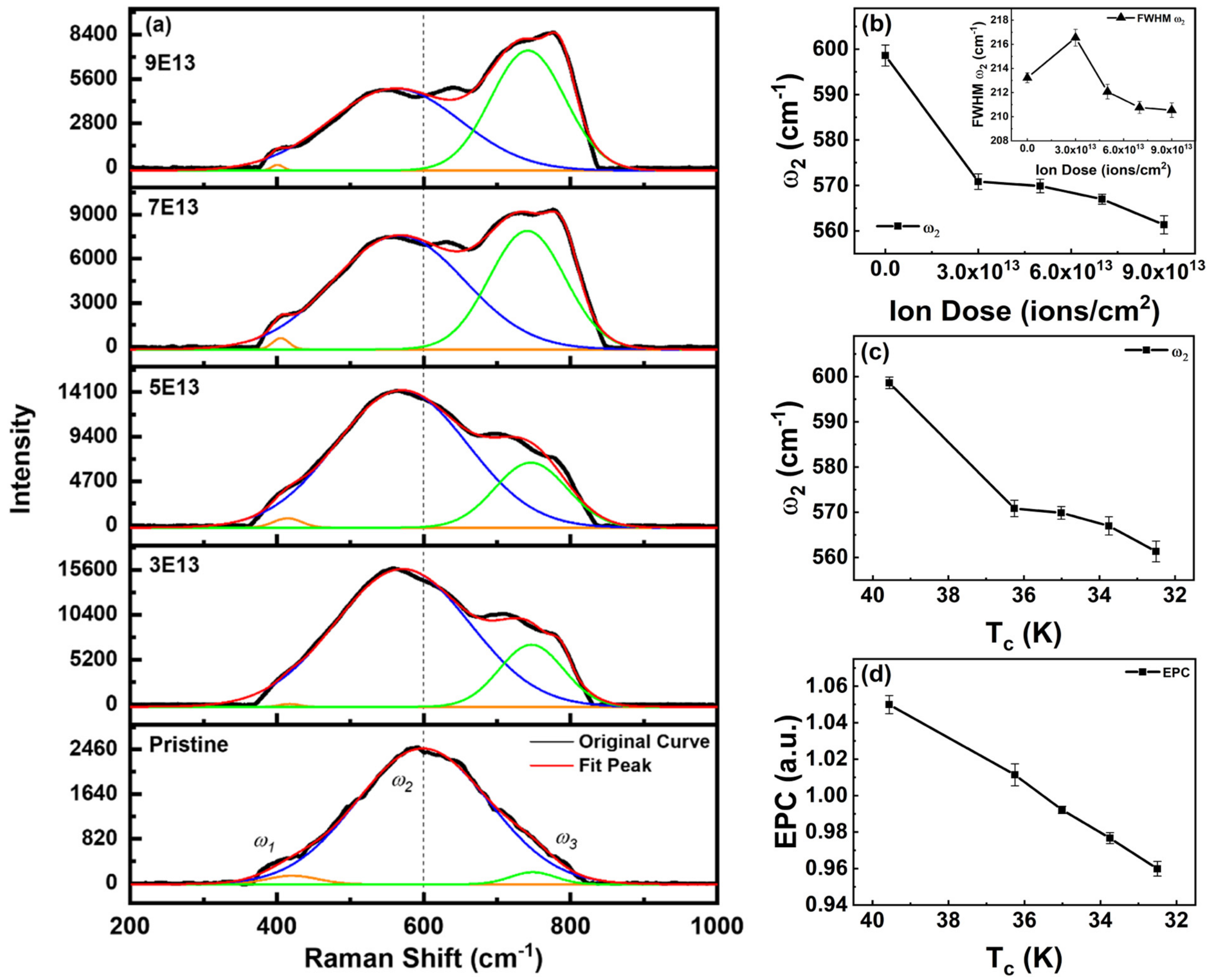

FIG. 4. (a) Raman spectra of the pristine and Ni-ion irradiated MgB_2 films. Three-mode fits using the Gaussian function of the E_{2g} (ω_2) and PDOS (ω_1 and ω_3) modes, (b) dependence of the Raman shift on the Ni-ion dose, and dependence of (c) the Raman shift and (d) electron–phonon coupling (EPC) on T_c.

be 1.02 and 0.45, respectively.[38,41,42] The results reveal that the superconductivity in both pristine and Ni-irradiated MgB_2 films is predominantly created by the σ-band. Ni-ion irradiation induces lattice distortions and defects, which weaken both the EPC and T_c. Furthermore, the Debye temperature (Θ_D) was found to decrease from 700.83 K for the pristine MgB_2 film to 666.07 K for the highest irradiated sample. These values agree with the reported range of 600–750 K for similar systems.[17,43]

Although the formation of defects and lattice disorders in Ni-ion-irradiated MgB_2 films suppressed the T_c of the MgB_2 film, they positively affected J_c. The field dependences of J_c at 5 and 20 K for both pristine and Ni-irradiated MgB_2 films are presented in Figs. 5(a) and 5(b). For the pristine MgB_2 films, the highest value of J_c was obtained at self-field and then generally decreased with increasing fields. Similar behaviors of J_c were also found for all Ni-irradiated MgB_2 films. The values of self-field Jc of all MgB_2 films at 5 K were lower than those at 20 K, and it was attributed to large flux jump due to thermal instability, which was like findings reported by Jung *et al.*[44] The effect of Ni-ion irradiation on J_c was then investigated. At low field regions, the J_c values of the Ni-irradiated MgB_2 films were lower than that of the pristine one. At 5 K, the J_c(B) curves of the 3×10^{13} and 5×10^{13} ions/cm^2-irradiated MgB_2 films were observed to cross that of the pristine one at 1.3 and 2.7 T, respectively. At 20 K, the crossover points were observed to be ∼2.5 T for both the 3×10^{13} and 5×10^{13} ions/cm^2-irradiated MgB_2 films. The observations of crossover points in the J_c(B) curves might reflect the contribution of different types of pinning centers in the MgB_2 films and will be discussed below. The J_c of the Ni-irradiated MgB_2 films was maintained $\sim 10^3$ A/cm^2 up to 5 T at 5 K and up to 3.7 T at 20 K. For power related applications, the value of J_c of 10^5 A/cm^2 has been required. In our work, the operation field for that Jc was found to be ∼4 T at 5 K and ∼3.2 T

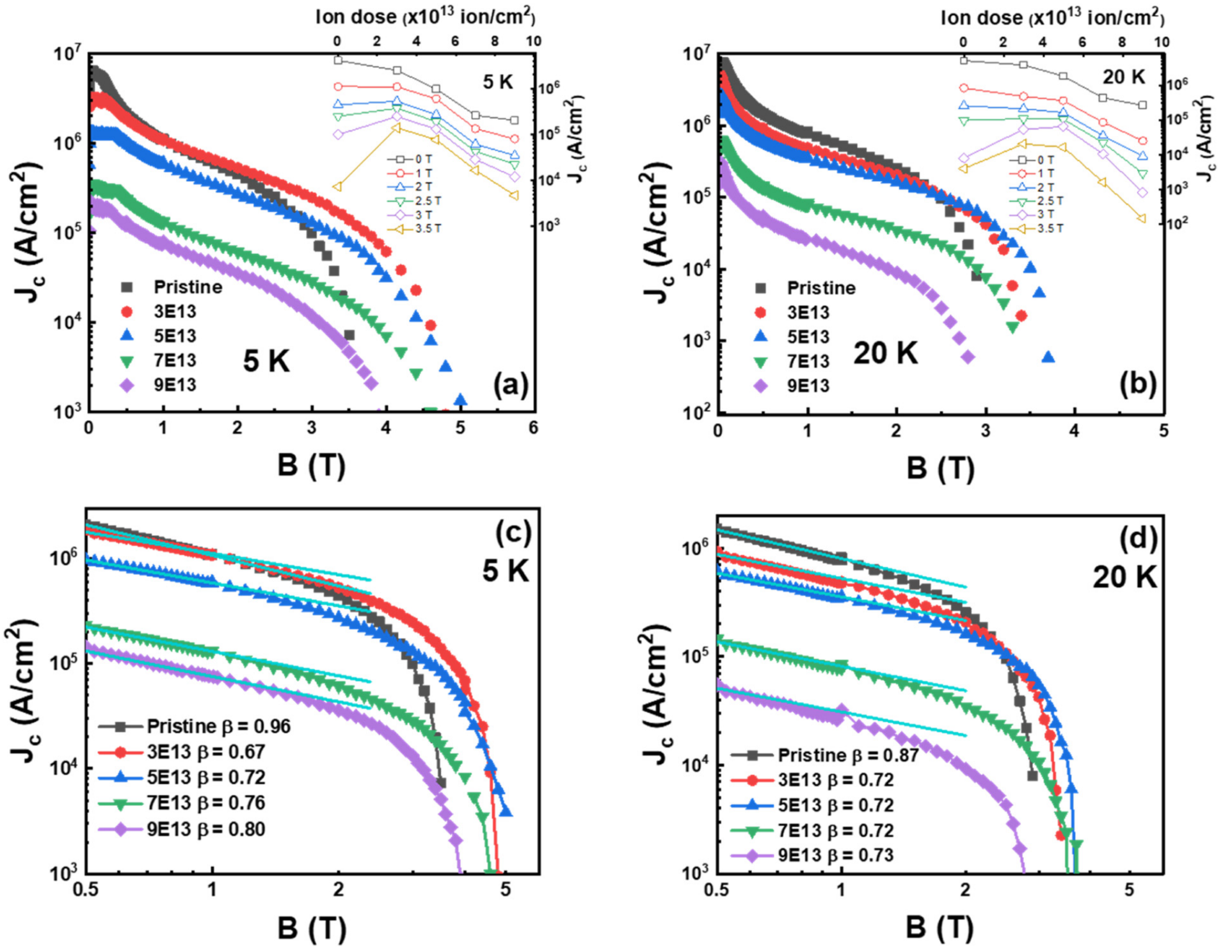

FIG. 5. J_c vs magnetic field of the pristine and Ni-ion irradiated MgB_2 films at (a) 5 and (b) 20 K and (c) and (d) a double logarithmic plot of data from (a) and (b) in which the power law $J_c \sim H^{-\beta}$ was applied in the intermediate field region. The inset of (a) and (b) showed variations of J_c with increasing the Ni-ion dose at different fields, in which the enhancements of J_c were observed at high field regions.

at 20 K. The Ni-ion irradiation enhanced J_c values in the high-field region for the 3×10^{13}, 5×10^{13}, and 7×10^{13} ions/cm^2 irradiated samples, likely due to the pinning effects of the induced defects. In comparison with a study on O-ion irradiation using the energy of ∼keV in which the O-ions were not completely penetrated throughout the films' thickness,[12] Ni-ion irradiation induced the stronger J_c enhancements of ∼1.5 times at both 5 and 20 K, which might reflect the advantage of using high energy for irradiation. In comparison with a study on Sn-ion irradiation using the energy ∼MeV,[8] the Ni-ion irradiation provided little lower J_c enhancement. A possible reason for this might be attributed to the magnetic property of Ni ion. Ni^{2+} was ferromagnetic ions, and there is a small amount of Ni^{2+} ions substituted into the MgB_2 crystal lattice. As a result, the superconductivity and J_c of the Ni-irradiated MgB_2 films were getting weakened as compared to those of the Sn-irradiated MgB_2 films. The inset of Figs. 5(a) and 5(b) showed the value of J_c for each Ni-ion dose at different fields. The J_c enhancements were clearly induced at high field region, which might reflect the role of additional pinning centers by Ni-ion irradiations.

To quantitatively analyze the J_c enhancements,[41] plots of J_c vs the magnetic field using the double-logarithmic scale are given in Figs. 5(c) and 5(d). Two distinct regimes may be classified. In the low-field region, where each vortex is individually pinned, the field independence of J_c indicates a single vortex pinning regime. In the intermediate field region, where vortex–vortex interactions dominate, J_c follows a field dependence of $J_c \approx H^{-\beta}$, where β represents the pinning strength.[15,45] At T = 5 K, β decreased from 0.96 for the pristine MgB_2 film to a minimum of 0.67 for the highest irradiated film. A similar trend was observed at T = 20 K. Theoretically, $\beta = 1$ characterizes weak pinning, while $\beta = 0.5$ is indicative of strong pinning.[46,47] The observed decrease in β

reveals a transition from weaker to stronger pinning mechanisms, likely due to the defects and disorder induced by Ni-ion irradiation.

The pinning nature in both pristine and Ni-irradiated MgB_2 films was also investigated. The pinning force density (F_p) was calculated from the field-dependent J_c data using the relation $F_p = B \times J_c$. In type-II superconductors, J_c and F_p typically decrease rapidly at the irreversibility field (B_{irr}), which is lower than the upper critical field (B_{c2}), and are extracted at $J_c = 1000\ A/cm^2$, as described by Jung *et al.*[45] As shown in Fig. 5, the values of B_{irr} were found to be comparable to those reported in previous studies on MgB_2 films fabricated using HPCVD,[8,45] which shows that the quality of the MgB_2 films in our work is consistent with previous reports. Hence, B_{irr} is used to define the reduced field b (where $b = B/B_{irr}$). Plots of the normalized pinning force density ($f_p = F_p/F_{p,max}$) as a function of the reduced field b for all samples are shown in Fig. 6.

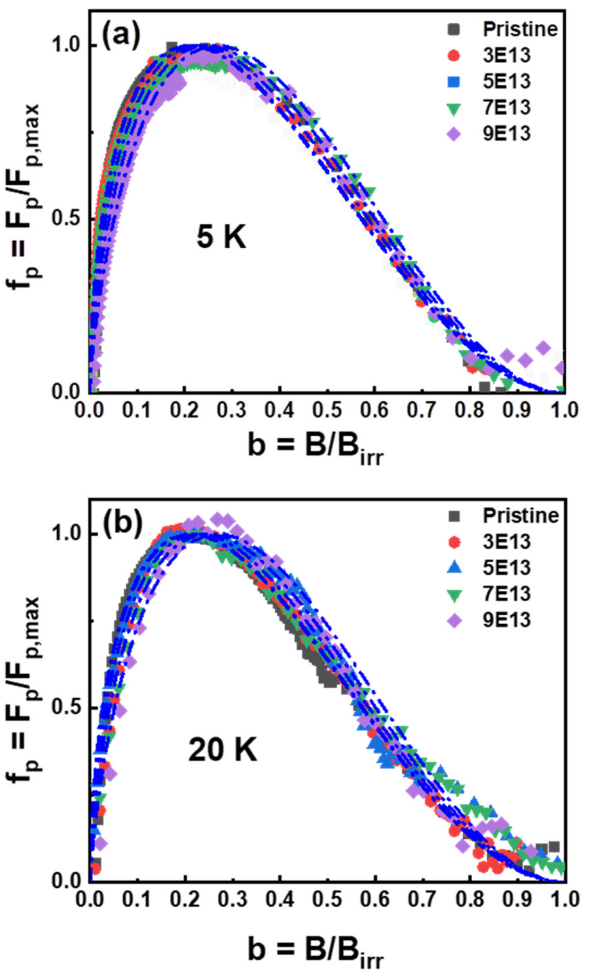

FIG. 6. Normalized volume pinning force f_p, $f_p = F_p/F_{p,max}$, on normalized field b, $b = B/B_{irr}$, the pristine and Ni-ion irradiated MgB_2 films at (a) 5 and (b) 20 K.

The scaling behaviors of flux pinning in MgB_2 films at both 5 and 20 K were analyzed using the Dew–Hughes model[48]

$$f_p = Ab^p(1-b)^q,$$

where A is a parameter independent of the applied field and p and q are the fitting parameters reflecting the type of pinning. The experimental data fit the theoretical model in the low field region. Values of p, q, and $b_{peak} = p/(p+q)$ were estimated. For all MgB_2 films at both 5 and 20 K, the value of q was consistently found to be 2, which may indicate the existence of core interaction.[11,46,48,49] This finding provided as solid evidence for the idea that a core interaction was the dominant interaction in type-II superconductors. The values of p and b_{peak} were then considered to identify the details of core pinning types in the MgB_2 films. At 5 K [Fig. 6(a)], p was approximately 0.53 and b_{peak} was around 0.21 for the pristine MgB_2 film, indicating that normal core surface pinning was dominant. The MgB_2 films fabricated by using the HPCVD method were nearly single crystalline, as confirmed by the XRD results. When the field was applied parallel to the *c*-axis of the films, grain boundaries effectively served as surface-pinning centers. For the Ni-irradiated MgB_2 films, which were irradiated with low ion doses (3×10^{13} and 5×10^{13} ions/cm^2), the values of p and b_{peak} slightly increased. However, for high ion doses (7×10^{13} and 9×10^{13} ions/cm^2), these values increased significantly to $p \approx 0.73$ and $b_{peak} \approx 0.27$. At 20 K [Fig. 6(b)], a similar trend was observed for p and b_{peak}, with thermal fluctuations contributing to the results.

According to the classification of Dew–Hughes, theoretical values of $p = 1$ and $q = 2$ correspond to normal point pinning. Previous studies show that normal point pinning in irradiated MgB_2 films is likely caused by distortion in the crystal structure, the lattice mismatch, or incomplete growth of superconducting grains.[15,45,46,50,51] In our study, the Ni ions penetrated the films, and the irradiation process generated point defects, such as ion tracks, and lattice distortions distributed homogeneously within the films. As a result, a partial shift from the normal surface to normal point pinning was achieved, leading to the coexistence of two pinning mechanisms in the 7×10^{13} and 9×10^{13} ions/cm^2-irradiated samples. The contributions of each type of pinning center were proposed by Higuchi *et al.*[51] and applied by Gajda *et al.*[52,53] The enhancements of J_c at low-field regions were predominantly due to surface pinning centers, while at middle and high-field regions, point pinning centers played a more significant role. This mechanism was likely responsible for the enhancement of J_c observed in Fig. 5. The point pinning centers, created by the irradiation process, were dominant in the Ni-irradiated MgB_2 films. These findings were consistent with the results in Fig. 6, where the fitting parameters of $p \approx 0.73$ and $b_{peak} \approx 0.27$ at high ion doses, although slightly deviating from theoretical values of $p = 1$ and $b_{peak} = 0.33$, confirm the major contribution of point pinning centers along with surface pinning centers.

Atomic force microscopy (AFM) was employed to probe the irradiation-driven morphological evolution of MgB_2 films, as shown in Fig. 7. After Ni-ion irradiation at a dose of 5×10^{13} atom/cm^2, the AFM images reveal a pronounced alteration in the grain boundary definition, accompanied by increased surface

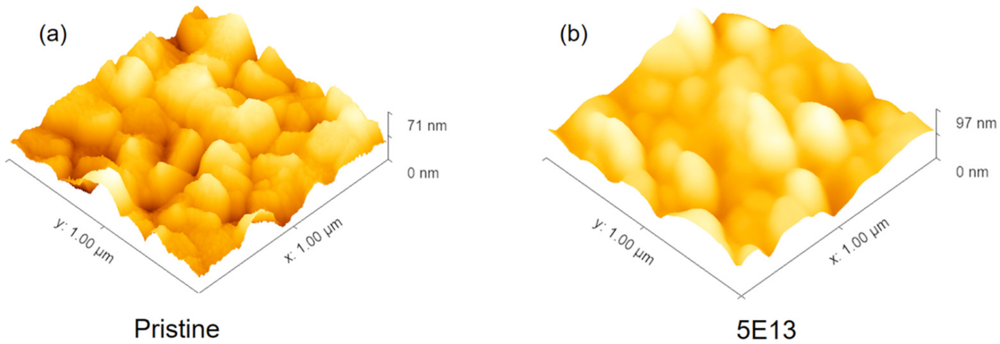

FIG. 7. Atomic force microscope (AFM) images of (a) a pristine film and (b) the Ni-irradiated MgB_2 films using the dose of 5×10^{13} atom/cm^2.

roughness. This reduction in grain boundary clarity denotes partial amorphization of the surface, consistent with irradiation-induced defect accumulation observed in other single-crystalline systems.[12] The modified grain morphology implies the formation of localized disordered regions, which could serve as effective flux pinning centers. While AFM is surface-sensitive and cannot resolve subsurface amorphization directly, the degradation of the grain boundary definition provides strong evidence for irradiation-induced structural disorder. These surface modifications are likely to contribute to enhanced vortex pinning, though their depth distribution and relation to bulk properties require further nanoscale characterization in future studies.

IV. CONCLUSIONS

Ni-ion irradiation of MgB_2 films induces notable lattice expansion, with the *c*-axis lattice constant increasing from 3.521 Å in pristine films to 3.550 Å at higher ion doses. This expansion is accompanied by crystallinity degradation, as reflected by the broadening of the (0002) XRD peak's FWHM from 0.257° to 0.479°. Williamson–Hall analysis further confirms increasing tensile strain with ion dose, which contributes to enhanced grain boundary pinning. The superconducting properties, however, are adversely affected; the critical temperature (T_c) decreases from 39.56 to 32.50 K at a dose of 9×10^{13} ions/cm^2, and electron–phonon coupling (EPC) weakens from 1.049 to 0.962, both indicative of lattice defects and disorder. The E_{2g} peak position in the Raman spectra shifted from 598 cm^{-1} (pristine) to 560 cm^{-1} (irradiated with 9×10^{13} ions/cm^2), showing increased lattice disorder. Additionally, the FWHM of the E_{2g} peak in the Raman spectra decreased from 213 cm^{-1} (pristine) to 198 cm^{-1}, partially linked to the T_c reduction. Despite the suppressed superconductivity, the critical current density (J_c) is enhanced in high magnetic fields for intermediate doses (3×10^{13} to 7×10^{13} ions/cm^2) due to defect-induced flux pinning. In low fields, J_c behavior aligns with single vortex pinning, transitioning to collective pinning at intermediate fields. Pinning strength (β) decreases from 0.96 to 0.67 at the highest dose, reflecting a shift toward stronger pinning mechanisms driven by irradiation defects. This is further supported by the calculated pinning force density and reduced field parameters that indicate transition toward point pinning at higher doses, enhancing J_c under strong fields. Atomic force microscopy reveals grain boundary degradation and increased surface roughness at doses around 5×10^{13} ions/cm^2, facilitating the formation of disordered regions that act as effective flux pinning centers.

ACKNOWLEDGMENTS

This research was funded by the Vietnam National Foundation for Science and Technology Development (NAFOSTED) under Grant No. 103.02–2023.78. J. Hwang acknowledges support from RS-2024-00460248 [from the National Research Foundation (NRF) of Korea]. S.-K. Chen would like to thank the Ministry of Higher Education (MoHE) Malaysia for their financial support through the Fundamental Research Grant Scheme (No. FRGS/1/2023/STG05/UPM/02/6). Ha H. Pham was funded by the Master, Ph.D. Scholarship Programme of Vingroup Innovation Foundation (VINIF) (Code VINIF.2024.TS.017).

AUTHOR DECLARATIONS

Conflict of Interest

The authors have no conflicts to disclose.

Author Contributions

Duong T. T. Nhan: Conceptualization (equal); Formal analysis (equal); Methodology (equal); Resources (equal); Writing – original draft (equal). **An T. Pham:** Formal analysis (equal); Resources (equal); Software (equal). **Tien Le:** Investigation (equal); Resources (equal); Software (equal). **Won-Nam Kang:** Investigation (equal); Resources (equal). **Dzung T. Tran:** Resources (equal); Software (equal). **Hong-Gu Lee:** Resources (equal). **Jungseek Hwang:** Investigation (equal); Resources (equal); Software (equal). **Nguyen Hoang Nam:** Resources (equal). **Ha H. Pham:** Resources (equal); Software (equal). **Khoi M. C. Pham:** Software (equal). **Pham Ngoc Thao:** Resources (equal); Software (equal). **Phan Hai:** Resources (equal); Software (equal). **Soo-Kien Chen:** Resources (equal). **M. Dogruer:** Investigation (equal); Resources (equal). **Kieu Xuan Thuy:** Resources (equal). **Duc H. Tran:** Conceptualization (equal); Data curation (equal); Funding acquisition (equal); Investigation (lead); Methodology (lead); Project administration (equal); Writing – review & editing (lead).

DATA AVAILABILITY

The data that support the findings of this study are available from the corresponding author upon reasonable request.

REFERENCES

[1] J. Nagamatsu, N. Nakagawa, T. Muranaka, Y. Zenitani, and J. Akimitsu, "Superconductivity at 39 K in magnesium diboride," Nature **410**, 63–64 (2001).
[2] D. Larbalestier, A. Gurevich, D. M. Feldmann, and A. Polyanskii, "High-T_c superconducting materials for electric power applications," Nature **414**, 368–377 (2001).
[3] M. Miryala, "Advancing sustainability: Magnesium-based solutions for environmental challenges and high-performance technologies in superconductivity," J. Magnes. Alloys **12**, 1257–1259 (2024).
[4] J. H. Durrell, M. D. Ainslie, D. Zhou, P. Vanderbemden, T. Bradshaw, S. Speller, M. Filipenko, and D. A. Cardwell, "Bulk superconductors: A roadmap to applications," Supercond. Sci. Technol. **31**, 103501 (2018).
[5] T. Le, D. T. Tran, H. G. Lee, W. S. Choi, J. Hwang, W. N. Kang, T. Park, T. Miyanaga, J. Yun, Y. Lee, J. Kim, P. Ngoc Thao, and D. H. Tran, "Influence of aluminum diffusion on MgB_2 films grown by hybrid physical–chemical vapor deposition using amorphous aluminum buffers," Results Phys. **58**, 107447 (2024).
[6] H. H. Pham, T. Le, T. N. Nguyen, N. H. Nam, N. T. Nguyen, M. K. Sohn, D. J. Kang, T. Park, J. Yun, Y. Lee, J. Kim, D. H. Tran, and W. N. Kang, "Correlation between electron-phonon coupling and superconductivity of Sn^{2+} ion irradiated MgB_2-thin films," Ceram. Int. **49**, 20586–20593 (2023).
[7] S.-G. Jung, S.-K. Son, D. Pham, W. C. Lim, J. Song, W. N. Kang, and T. Park, "Influence of carbon-ion irradiation on the superconducting critical properties of MgB_2 thin films," Supercond. Sci. Technol. **34**, 129501 (2021).
[8] T. Le, H. H. Pham, N. T. Nghia, N. H. Nam, T. Miyanaga, D. H. Tran, and W. N. Kang, "Effects of Sn-ion irradiation on local structure and flux pinning properties of MgB_2 thin films," Ceram. Int. **49**, 2715–2720 (2023).
[9] G. K. Perkins, Y. Bugoslavsky, A. D. Caplin, J. Moore, T. J. Tate, R. Gwilliam, J. Jun, S. M. Kazakov, J. Karpinski, and L. F. Cohen, "Effects of proton irradiation and ageing on the superconducting properties of single crystalline and polycrystalline MgB_2," Supercond. Sci. Technol. **17**, 232 (2003).
[10] M. Putti, R. Vaglio, and J. M. Rowell, "Radiation effects on MgB_2: A review and a comparison with A15 superconductors," Supercond. Sci. Technol. **21**, 043001 (2008).
[11] J. Wang, C. G. Zhuang, J. Li, Z. W. Wu, S. Li, H. F. Chu, Q. R. Feng, and D. N. Zheng, "Enhancement of critical current density and flux pinning in oxygen ion-irradiated MgB_2 thin films," Supercond. Sci. Technol. **22**, 045020 (2009).
[12] D. Pham, S.-G. Jung, D. H. Tran, T. Park, and W. N. Kang, "Effects of oxygen ion implantation on single-crystalline MgB_2 thin films," J. Appl. Phys. **125**, 023904 (2019).
[13] R. P. Putra, J. Y. Oh, M. Angga Anugrah, T. Miyanaga, and B. Kang, "Evidence of disordered local structure of ZnO buffered MgB_2 films via polarized extended x-ray absorption fine structure analysis," Appl. Surf. Sci. **663**, 160210 (2024).
[14] R. Gandikota, R. K. Singh, J. Kim, B. Wilkens, N. Newman, J. M. Rowell, A. V. Pogrebnyakov, X. X. Xi, J. M. Redwing, S. Y. Xu, Q. Li, and B. H. Moeckly, "Effect of damage by 2 MeV He ions and annealing on H_{c2} in MgB_2 thin films," Appl. Phys. Lett. **87**, 072507 (2005).
[15] S. G. Jung, S. K. Son, D. Pham, W. N. Kang, W. C. Lim, J. Song, and T. Park, "Enhanced critical current density in the carbon-ion irradiated MgB_2 thin films," J. Phys. Soc. Jpn. **88**, 034716 (2019).
[16] D. Pham, S. G. Jung, D. H. Tran, T. Park, and W. N. Kang, "Angle-dependent Hall effect and vortex dynamics in single-crystalline MgB_2 thin films," Supercond. Sci. Technol. **32**, 115011 (2019).
[17] D. T. Tran, T. Le, Y. S. Seo, D. H. Tran, T. Park, S. G. Jung, T. Miyanaga, C. Kim, S. Yeo, W. N. Kang, and J. Hwang, "Roles of Fe-ion irradiation on MgB_2 thin films: Structural, superconducting, and optical properties," J. Alloys Compd. **968**, 172144 (2023).
[18] J. F. Ziegler and J. P. Biersack, "The stopping and range of ions in matter," in *Treatise on Heavy-Ion Science* (Springer Nature, 1985), pp. 93–129.
[19] J. F. Ziegler, M. D. Ziegler, and J. P. Biersack, "SRIM—The stopping and range of ions in matter," Nucl. Instrum. Methods Phys. Res. B **268**, 1818–1823 (2010).
[20] H. J. Kim, W. N. Kang, E. M. Choi, M. S. Kim, K. H. P. Kim, and S. I. Lee, "High current-carrying capability in *c*-axis-oriented superconducting MgB_2 thin films," Phys. Rev. Lett. **87**, 087002 (2001).
[21] D. T. Tran, T. Le, H. G. Lee, T. Park, N. T. Nghia, B. T. Hoa, D. H. Tran, W. N. Kang, and J. Hwang, "Infrared spectroscopic study on Nb-ion-irradiated MgB_2 thin films," Curr. Appl. Phys. **66**, 30–34 (2024).
[22] R. P. Putra, J.-Y. Oh, M. Angga Anugrah, T. Miyanaga, and B. Kang, "Evidence of disordered local structure of ZnO buffered MgB_2 films via polarized extended x-ray absorption fine structure analysis," Appl. Surf. Sci. **663**, 160210 (2024).
[23] T. Takenobu, T. Ito, D. Hieu Chi, K. Prassides, and Y. Iwasa, "Intralayer carbon substitution in the MgB_2 superconductor," Phys. Rev. B **64**, 134513 (2001).
[24] A. F. Goncharov, V. V. Struzhkin, E. Gregoryanz, J. Hu, R. J. Hemley, H. Mao, G. Lapertot, S. L. Bud'ko, and P. C. Canfield, "Raman spectrum and lattice parameters of MgB_2 as a function of pressure," Phys. Rev. B **64**, 100509 (2001).
[25] S. Lee, T. Masui, A. Yamamoto, H. Uchiyama, and S. Tajima, "Carbon-substituted MgB_2 single crystals," Phys. C **397**, 7–13 (2003).
[26] T. Yildirim, O. Gülseren, J. W. Lynn, C. M. Brown, T. J. Udovic, Q. Huang, N. Rogado, K. A. Regan, M. A. Hayward, J. S. Slusky, T. He, M. K. Haas, P. Khalifah, K. Inumaru, and R. J. Cava, "Giant anharmonicity and nonlinear electron-phonon coupling in MgB_2: A combined first-principles calculation and neutron scattering study," Phys. Rev. Lett. **87**, 37001 (2001).
[27] K. Kunc, I. Loa, K. Syassen, R. K. Kremer, and K. Ahn, "MgB_2 under pressure: Phonon calculations, Raman spectroscopy, and optical reflectance," J. Phys.: Condens. Matter **13**, 9945–9962 (2001).
[28] J. Hlinka, I. Gregora, J. Pokorný, A. Plecenik, P. Kúš, L. Satrapinsky, and Š. Beňačka, "Phonons in MgB_2 by polarized Raman scattering on single crystals," Phys. Rev. B **64**, 140503 (2001).
[29] J. Wang, C. G. Zhuang, J. Li, Y. Z. Wang, Q. R. Feng, and D. N. Zheng, "Upper critical field and Raman spectra of MgB_2 thin films irradiated with low energy oxygen ion," J. Appl. Phys. **106**, 093915 (2009).
[30] P. Postorino, A. Congeduti, P. Dore, A. Nucara, A. Bianconi, D. D. Castro, S. De Negri, and A. Saccone, "Effect of the Al content on the optical phonon spectrum in $Mb_{1-x}Al_xB_2$," Phys. Rev. B **65**, 20507 (2001).
[31] K. A. Yates, Burnell, N. A. Stelmashenko, D.-J. Kang, H. N. Lee, B. Oh, and M. G. Blamire, "Disorder-induced collapse of the electron-phonon coupling in MgB_2 observed by Raman spectroscopy," Phys. Rev. B **68**, 220512 (2003).
[32] J. Arvanitidis, K. Papagelis, K. Prassides, G. A. Kourouklis, S. Ves, T. Takenobu, and Y. Iwasa, "Raman spectroscopic study of carbon substitution in MgB_2," J. Phys. Chem. Solids **65**, 73–77 (2004).
[33] K.-P. Bohnen, R. Heid, and B. Renker, "Phonon dispersion and electron-phonon coupling in MgB_2 and AlB_2," Phys. Rev. Lett. **86**, 5771–5774 (2001).
[34] R. Osborn, E. A. Goremychkin, A. I. Kolesnikov, and D. G. Hinks, "Phonon density of states in MgB_2," Phys. Rev. Lett. **87**, 17005 (2001).
[35] W. X. Li, Y. Li, R. H. Chen, R. Zeng, S. X. Dou, M. Y. Zhu, and H. M. Jin, "Raman study of element doping effects on the superconductivity of MgB_2," Phys. Rev. B **77**, 94517 (2008).
[36] T. Le, D. T. Tran, H. G. Lee, W. S. Choi, J. Hwang, W. N. Kang, T. Park, T. Miyanaga, J. Yun, Y. Lee, J. Kim, P. Ngoc Thao, and D. H. Tran, "Influence of aluminum diffusion on MgB_2 films grown by hybrid physical–chemical vapor deposition using amorphous aluminum buffers," Results Phys. **58**, 107447 (2024).
[37] W. L. McMillan, "Transition temperature of strong-coupled superconductors," Phys. Rev. **167**, 331–344 (1968).

[38]J. Kortus, I. I. Mazin, K. D. Belashchenko, V. P. Antropov, and L. L. Boyer, "Superconductivity of metallic boron in MgB_2," Phys. Rev. Lett. **86**, 4656–4659 (2001).
[39]I. N. Askerzade, A. Gencer, and N. Güçlü, "On the Ginzburg-Landau analysis of the upper critical field H_{c2} in MgB_2," Supercond. Sci. Technol. **15**, L13–L16 (2002).
[40]A. Brinkman, A. A. Golubov, H. Rogalla, O. V. Dolgov, J. Kortus, Y. Kong, O. Jepsen, and O. K. Andersen, "Multiband model for tunneling in MgB_2 junctions," Phys. Rev. B **65**, 180517 (2002).
[41]X. K. Chen, M. J. Konstantinović, J. C. Irwin, D. D. Lawrie, and J. P. Franck, "Evidence for two superconducting gaps in MgB_2," Phys. Rev. Lett. **87**, 157002 (2001).
[42]W. X. Li, R. H. Chen, Y. Li, M. Y. Zhu, H. M. Jin, R. Zeng, S. X. Dou, and B. Lu, "Raman study on the effects of sintering temperature on the Jc(H) performance of MgB_2 superconductor," J. Appl. Phys. **103**, 013511 (2008).
[43]M. A. Susner, M. D. Sumption, A. Takase, and E. W. Collings, "Evidence for Zr site-substitution for Mg in PLD-deposited MgB_2 thin films," Supercond. Sci. Technol. **27**, 075009 (2014).
[44]S.-G. Jung, Y. Han, J. H. Kim, R. Hidayati, J.-S. Rhyee, J. M. Lee, W. N. Kang, W. S. Choi, H.-R. Jeon, J. Suk, and T. Park, "High critical current density and high-tolerance superconductivity in high-entropy alloy thin film," Nat. Commun. **13**, 3373 (2022).
[45]S. G. Jung, D. Pham, J. M. Lee, Y. Han, W. N. Kang, and T. Park, "Effects of surface damage on critical current density in MgB_2 thin films," Curr. Appl. Phys. **22**, 14–19 (2021).
[46]S.-G. Jung, W. K. Seong, and W. N. Kang, "Flux pinning mechanism in single-crystalline MgB_2 thin films," J. Phys. Soc. Jpn. **82**, 114712 (2013).
[47]B. Dam, J. M. Huijbregtse, F. C. Klaassen, R. C. F. Van Der Geest, G. Doornbos, J. H. Rector, A. M. Testa, S. Frelsem, J. C. Martinez, B. Stäuble-Pümpin, and R. Griessen, "Origin of high critical currents in $YBa_2Cu_3O_{7-\delta}$ superconducting thin films," Nature **399**, 439–442 (1999).
[48]D. Dew-Hughes, "Flux pinning mechanisms in type II superconductors," Philos. Mag. **30**, 293–305 (1974).
[49]X. Shi, K. Pradhan, M. Tokunaga, K. Yamazaki, T. Tamegai, Y. Takano, K. Togano, H. Kito, and H. Ihara, "Flux-pinning properties of single crystalline and dense polycrystalline MgB_2," Phys. Rev. B **68**, 104514 (2003).
[50]R. P. Putra, Y. S. Lee, J. Y. Oh, L. M. Tien, W. N. Kang, T. Miyanaga, and B. Kang, "Correlation between Tc and local structure of MgB_2 with ZnO buffer layer: X-ray absorption fine structure study," Phys. B **645**, 414234 (2022).
[51]T. Higuchi, S. I. Yoo, and M. Murakami, "Comparative study of critical current densities and flux pinning among a flux-grown $NdBa_2Cu_3O_y$ single crystal, melt-textured Nd–Ba–Cu–O, and Y–Ba–Cu–O bulks," Phys. Rev. B **59**, 1514 (1999).
[52]D. Gajda, A. Morawski, A. J. Zaleski, W. Häßler, K. Nenkov, M. Małecka, M. A. Rindfleisch, M. S. A. Hossain, and M. Tomsic, "Experimental research of high field pinning centers in 2% C doped MgB_2 wires at 20 K and 25 K," J. Appl. Phys. **120**, 113901 (2016).
[53]D. Gajda, "Analysis method of high-field pinning centers in NbTi wires and MgB_2 wires," J. Low Temp. Phys. **194**, 166–182 (2019).